Monitoring temporal variability of bubble release at seeps: The hydroacoustic swath system GasQuant

Jens Greinert[1,2]

Received 20 December 2007; accepted 14 May 2008; published 30 July 2008.

[1] A lander-based hydroacoustic swath system, GasQuant, was deployed in an intensely bubbling seep area at the shelf west of the Crimea Peninsula, Black Sea. With its horizontally oriented swath (21 beams, 63° swath angle, 180 kHz) GasQuant operates in a sonar-like mode and monitors bubbles remotely, exploiting their strong backscattering when crossing the swath. All active seep spots were monitored simultaneously within the covered area (2075 m^2). Even applying simple processing and visualization techniques (moving average for filtering, FFT for spectrum analyses; swath and trace plots) identified 17 seeps of different activity patterns that have been grouped as follows: (1) sporadically active with one to a few long bursts (up to 18 min) or randomly occurring short bursts (<200 bursts and active for <5% of the observation time); (2) regularly active seeps showing mainly short bursts of less than one minute but also longer burst of a few minutes (200–350 bursts and 5 to 20% active); (3) frequently active spots with sometimes very periodic bubble release (>350 bursts or >20% active). Studying the bubble release variability of single seeps and of the entire area allows speculation about the external and internal processes that modulate the bubble release. In the study area none of the 17 seeps was found to be permanently active. Only one was active for 75% and another one for 45% of the time monitored. The rest only released bubbles during less than 20% of the time with an overall average of only 12%. This would have strong implications for flux extrapolations if these were based on very accurate but few short-term measurements. Both strong overestimates and underestimates are possible. High-resolution monitoring over at least one tidal cycle as with the GasQuant system might help to get an idea of the temporal variability. Thus flux extrapolations can be corrected to better reflect the real seep activity.

Citation: Greinert, J. (2008), Monitoring temporal variability of bubble release at seeps: The hydroacoustic swath system GasQuant, *J. Geophys. Res.*, *113*, C07048, doi:10.1029/2007JC004704.

1. Introduction

[2] Methane bubble release in marine or lacustrine environments is a common phenomenon around cold seeps, which may be related to gas hydrate deposits, mud volcanoes, pockmarks or a mixture of those [*Suess et al.*, 1999; *Leifer and Judd*, 2002; *Van Rensbergen et al.*, 2002; *Torres et al.*, 2002; *Sauter et al.*, 2006; *Greinert et al.*, 2006]. It is proposed that massive gas hydrate decomposition played an important role in past atmospheric CH_4 budgets and climate change [*Dickens et al.*, 1995; *Norris and Röhl*, 1999; *Kennett et al.*, 2003]. Despite the fact that methane from continuous or sporadically, gently bubbling seeps will dissolve rapidly in the water column [*Leifer and Patro*, 2002; *McGinnis et al.*, 2006], massive bubble release that creates upwelling and forms a bubble plume can transport significant amounts of methane into the atmosphere [*Leifer et al.*, 2006]. Unfortunately, such bubble eruptions are difficult to study as they are transient and highly intermittent. Most described bubbling seeps are not as vigorously active as those described by *Leifer et al.* [2006] and show bubble release as single or multiple bubble trains or the release of bubble clouds in an eruptive manner [e.g., *Hornafius et al.*, 1999; *Dimitrov*, 2002; *Leifer and MacDonald*, 2003; *Sauter et al.*, 2006]. This is also true for the seeps described here, but the large abundance of seep sites (that combine several bubble releasing holes on a meter scale) was the reason to classify this study area as very active [*Naudts et al.*, 2006].

[3] Little is known about the temporal variability at seeps for both bubble and fluid release. Only a limited number of successful attempts have been carried out to measure bubble fluxes but most efforts lack detailed information about the temporal variability over a longer time with a resolution less than 1 h. There are several reasons for this, such as technical limitations for data storage for video/photo observations [e.g., *MacDonald et al.*, 2005]; time restrictions for submersible/scuba diving experiments [e.g., *Sauter et al.*, 2006;

[1]Leibniz-Institute of Marine Science, Kiel, Germany.
[2]Now at Renard Centre of Marine Geology, Ghent University, Gent, Belgium.

0148-0227/08/2007JC004704

Leifer et al., 2006]; or time constraints for ship-based hydroacoustic single beam surveys [*Hornafius et al.*, 1999; *Heeschen et al.*, 2003; *Greinert et al.*, 2006].

[4] For most measurements and observations, periodic, cyclic, pulsing or transient seep activity is reported. *Leifer et al.* [2004] points out that seep activity occurs on different timescales ranging from decadal or tidal to subhourly periods. Reasons for this are external forcing by tides, swells, changing bottom current conditions [e.g., *Linke et al.*, 1999; *Tryon et al.*, 1999; *Quigley et al.*, 1999; *Tryon et al.*, 2002]; man-made changes (e.g., water table changes for fresh water seeps [*Wever et al.*, 2006]) or large-scale geological events like earthquakes [*Obzhirov et al.*, 2004]. Internal variations of the gas pressure and finally the gas supply that fills small reservoirs close to the actual bubble vent may cause these vents, seep sites or entire seep areas to be active in a geyser-like manner. Gaining knowledge about this variability and activity changes might provide insights into the mechanisms that cause and trigger seepage.

[5] For studying the spatial and temporal variability of bubble release, remote monitoring of the area in question is essential. Important requirements are that the monitoring device does not change the very sensitive fluid system and its environmental parameters. The system should cover a wide area at the same time to record several bubbling spots simultaneously and should be able to take measurements over several days to weeks with a resolution of a few seconds. The system must be sensitive enough to detect very few bubbles in decimeter resolution even in several tens of meters distance to monitor the spatial variability.

[6] This task cannot be carried out with video systems or other single spot measuring devices unless all possible bubbling sites are monitored using several systems simultaneously. Contrary to that, hydroacoustic is very sensitive for detecting bubbles owing to the strong impedance of gas bubbles in water [*Medwin and Clay*, 1998]. Deployed far away, even heavy, large lander-based systems will not interfere with the seep system. Hydroacoustic systems can cover a wide area simultaneously and monitor it over a long time. Thus they are an ideal method for studying the temporal variability of submarine bubble release in a predefined area.

[7] For this study, an existing multibeam system (Seabeam 1000) was converted and can now be deployed under video guidance as a remote-working, in situ monitoring system in close proximity to active gas seepage areas. In the following, the system called GasQuant will be described and data from a shelf area in the Black Sea showing different release patterns and periodicities of bubble release are presented.

2. Study Area

[8] The CRIMEA project focused on the shelf west of the Crimea Peninsula in the Black Sea during two cruises in 2003 and 2004 (Figure 1). In this area, seepage was first discovered more than 10 years ago [*Polikarpov et al.*, 1989]. The area was repeatedly and densely mapped by single beam echosounder surveys during CRIMEA. A detailed description of the occurrence and relation between bubble seep spots, seafloor morphology and subbottom structures is presented by *Naudts et al.* [2006]. On the basis of this information GasQuant was deployed in the right distance and facing toward active seeps from 17 to 20 June 2004 in ~92 m water depth. This water depth contributes to near-ideal hydroacoustic conditions as disturbing signals from fish do not occur anymore as the Black Sea becomes anoxic below 120 m and oxygen is already drastically reduced to less than 3 mg/L in 92m water depth [*McGinnis et al.*, 2006]. The almost flat seafloor reduces the possibility of scattering from the bottom.

[9] ADCP measurements undertaken two days before the GasQuant deployment during another lander operation show currents typically around 20cm/s (Figure 2). No oscillating current variations are visible in this data set but have been observed during measurements in 2003 and, at a greater depth, in 2004. To avoid any hydroacoustic interference, ADCP measurements were not undertaken during the GasQuant deployment itself. Visual observations during submersible dives with JAGO (RV *POSEIDON*, 317–1, October 2004; METROL Project) confirmed the strong bottom currents and showed that bubbles are of mm size with diameters ranging from 4 to 11 mm (mean about 6 mm) in the study area.

3. Methods

3.1. GasQuant System

[10] GasQuant uses the fact that even very small bubbles can be easily detected by hydroacoustics owing to their strong impedance difference to water which results in strong backscattering of the transmitted acoustic pulse. This is also true if bubbles occur in great distances from the transducer (depending on the frequency used) and if they are not in resonance with the used frequency and the ambient pressure. In fact, the frequency of GasQuant (180 kHz) was chosen to avoid resonance effects at the expected bubble size distribution (~1 mm to 20 mm in diameter) and the pressure in up to 1000 m water depth [*Greinert and Nützel*, 2004] (1000 m is the depth rating of the used transducer). At the pressure of the hydroacoustic swath in this study (89 m water depth) a bubble of 115 μm in diameter would become resonant at 180 kHz. During experiments in a dry dock [*Greinert and Nützel*, 2004], the system proved to give a detectable amplitude increase if two bubbles (4 to 7mm diameter) cross the swath at one spot. Although flux quantifications are possible as outlined by *Greinert and Nützel* [2004], the system used in the Black Sea in June 2004 could not be calibrated properly to provide real flux measurements. Nevertheless it allowed very accurate monitoring of the spatial distribution, the temporal variability and relative flux differences between seeps.

[11] GasQuant is based on a 'normal' multibeam Seabeam 1000 system which was modified by L3-Communication ELAC-Nautik (Kiel, Germany) to run as a stand-alone system operating in a sonar-like mode. The main difference to a seafloor-mapping multibeam system is the horizontal orientation of the swath. The swath consists of 21 beams with 1.5° vertical and 3° horizontal beam width, covering a total swath angle of 63° (Figure 3). The transducer is mounted onto a cardanic frame that keeps the hydroacoustic swath horizontal even if the lander is slightly tilted. The transducer is fixed at ~3 m above the seafloor. With a

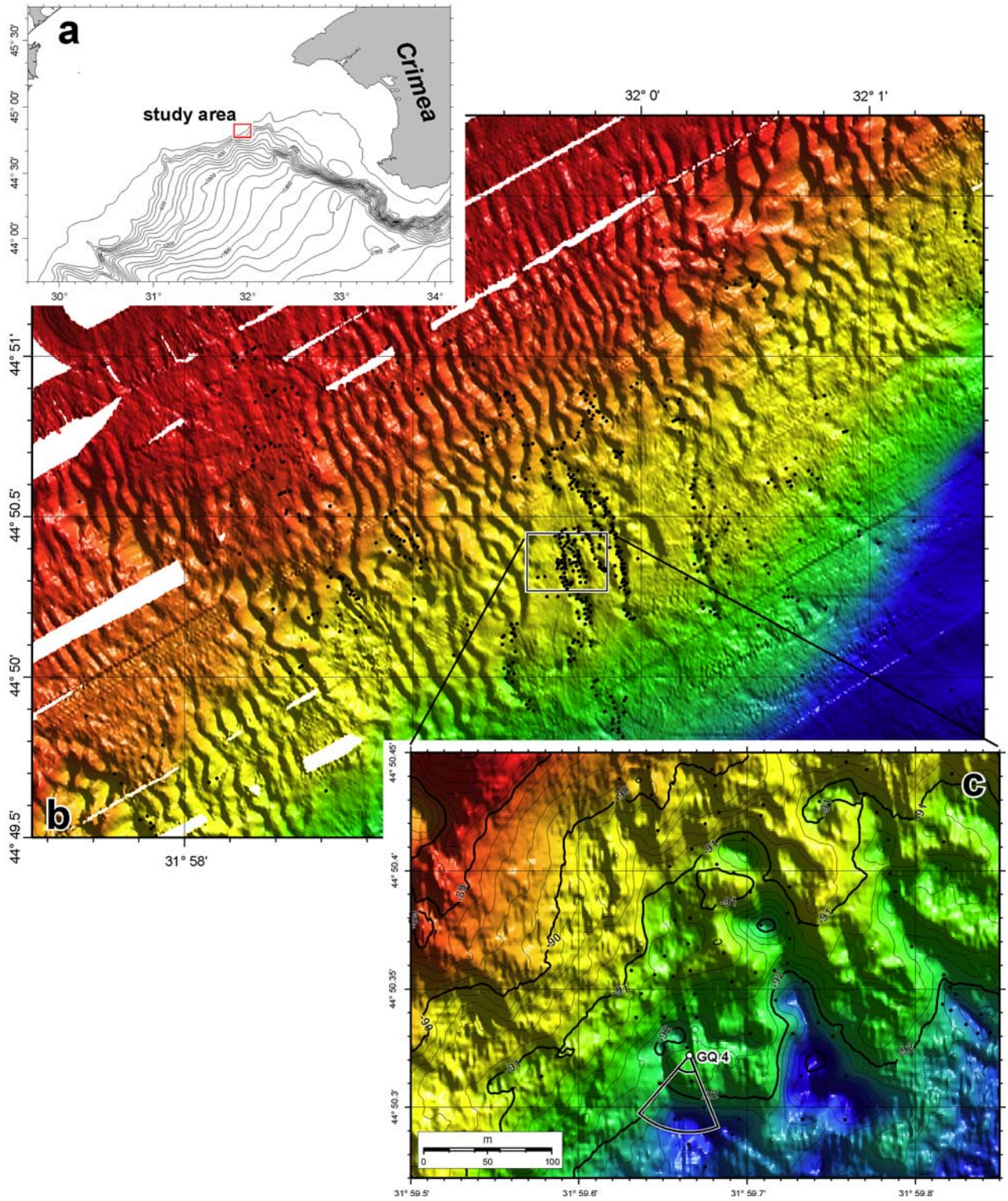

Figure 1. (b) Bathymetric map of (a) the study area west of the Crimea Peninsula, Black Sea. Black dots mark bubble release spots detected by single beam echosounder (Figures 1b and 1c). (c) Position and ping direction of GasQuant during the deployment (GQ4) within a highly active seep area. Contour lines every 20 cm; lines annotated every meter.

vertical beam angle of 1.5°, the signal hits the seafloor in more than 200 m distance.

[12] A modified version of HydrostarOnline was used as recording software (standard multibeam recording software for Seabeam 1000 series). The received signal is converted from analog to digital every 128 μs; this corresponds to a water cell thickness of 9.6 cm (at 1500 m/s sound velocity) along the beam (lateral resolution) for one data sample.

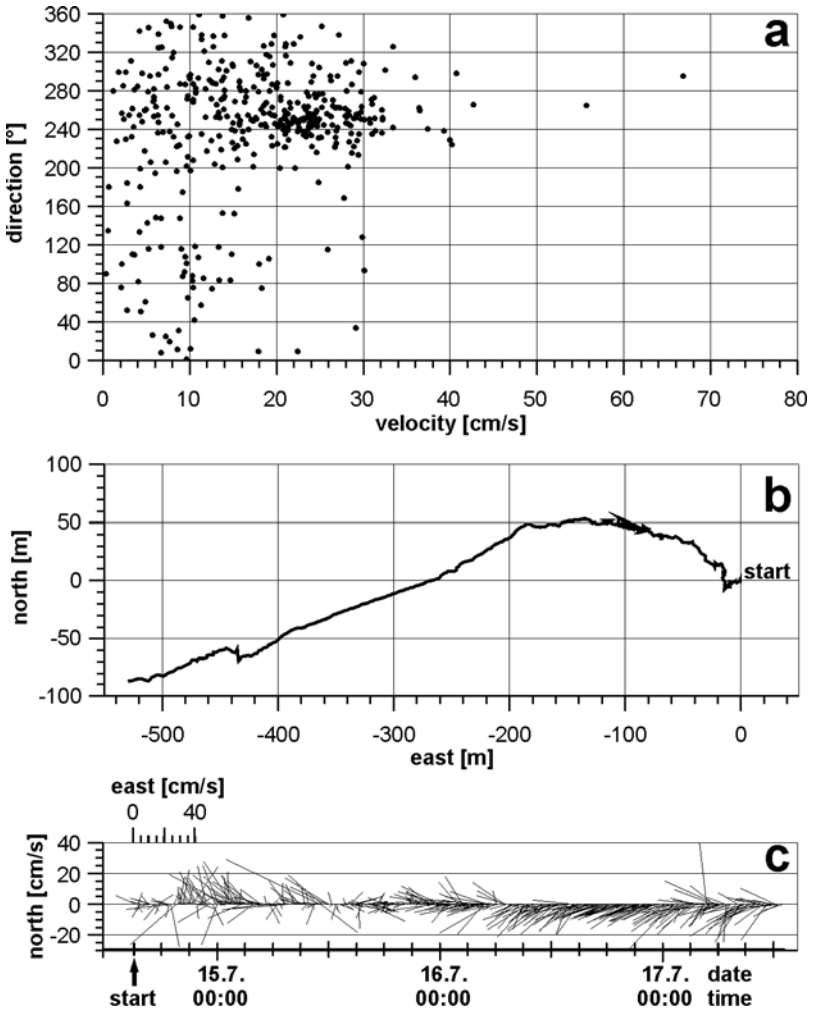

Figure 2. ADCP measurements have been performed during a lander deployment 2 days before the GasQuant recording started (ADCP setting: 75 kHz; 10-min interval, 250 bursts per interval, 80-cm bin length). The data shown represent the currents in 85 m water depth 400 m away from the GasQuant station from 14 June 2004, 1500 local time, to 17 June 2004, 1200 local time. Figures 2a and 2c show velocities between 20 to 30 cm/s are common and that the main current direction is toward the SW (240°, shown in Figures 2a and 2b). (c) Changing currents displayed as vectors for each burst.

During the measurements, the pulse length was 1ms and the ping rate was 4 s. With 1 ms pulse length and a 128 μs sampling rate, the data are oversampled as will be shown later. The signal is TVG-corrected (time varied gain), automatically gain adjusted (for a better dynamic performance of the received signal) and finally stored as raw data. All in all, 512 samples are recorded for each beam covering a distance between 14 and 63 m away from the transducer. This results in a total of 10,752 cells (512 samples by 21 beams) that were recorded, monitoring an area of 2075 m^2 for each ping.

[13] The GasQuant lander system is video guided when being deployed [*Pfannkuche and Linke*, 2003]. The direction in which the system will ping is video-monitored by one of the launcher cameras during the deployment by looking at a compass fixed to the lander frame. At the seafloor, GasQuant takes measurements following a preprogrammed routine for a defined period before it goes into a sleep mode without pinging to save energy. During the deployment of 55 h 23 min, the setting was ~1 h pinging followed by a ~15-min sleep period. A few longer gaps occur in the data set owing to longer restart periods.

3.2. Basic Data Processing

[14] Data are stored in binary xse format, for which L3-Communication ELAC-Nautik provides a full description. A self-written software package extracted the needed data and provided processing, visualization and export possibilities for analysis. The aim of the data processing was to identify bubble-releasing seep positions in the data and to study the temporally variable release activity for both single seeps and the entire seep area. The activity of a seep at a certain position is given by the signal strength changes over time (in the following called 'trace') in the respective cell(s).

[15] Different filters were tested to enhance the signal-to-noise ratio, to smooth traces for visualization and seep

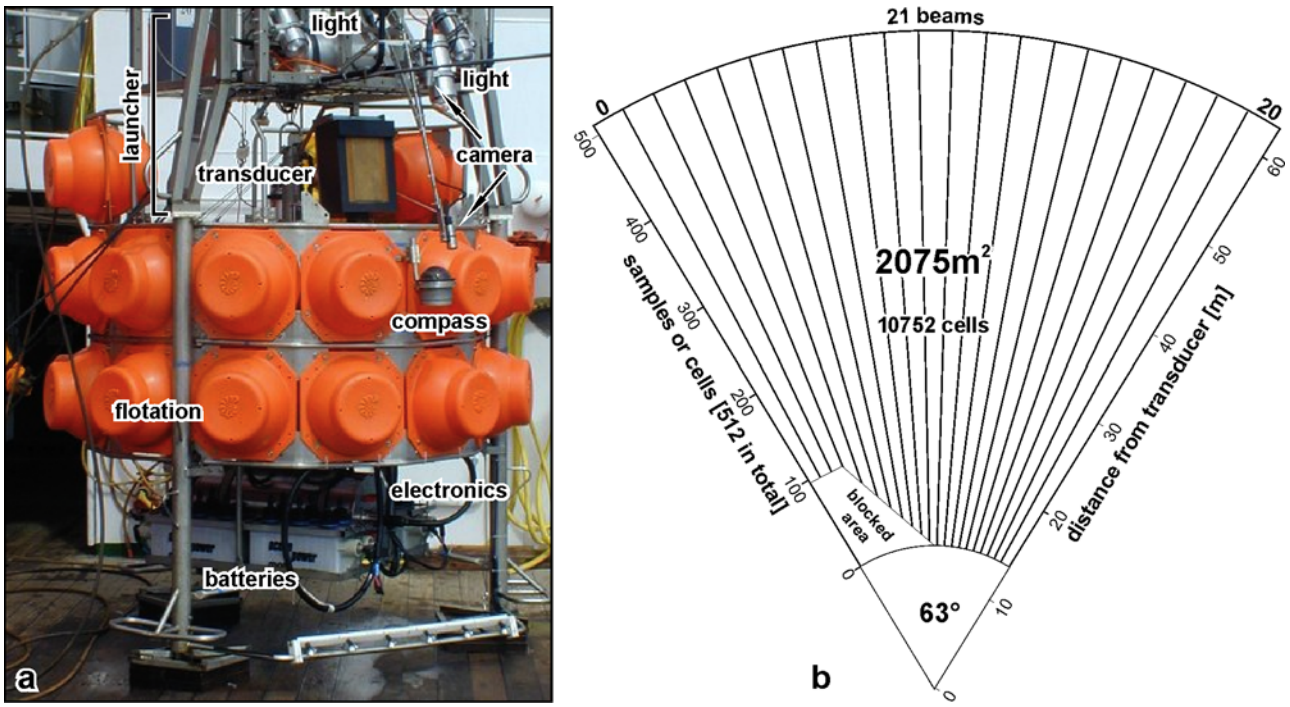

Figure 3. (a) Image of the GasQuant lander with launcher system ready for deployment. The lander is video-guided while being towed over the seafloor. Several lights and two cameras (one monitoring the compass) secure safe and exact positioning on the seafloor relative to the target area. (b) Size of the hydroacoustic swath showing the 21 beams and positions of the analyzed samples per beam. Owing to the block depth setting of the system (a relic of its swath mapping history), no correct data have been recorded from the blocked area.

activity calculations, or to correct low-frequency background variations over time. To smooth traces simple moving average calculations = boxcar match filter (the sudden begin and end of a bubble burst matches a boxcar filter kernel), as well as band-pass filtering using Fast Fourier Transformation (FFT, applying different filter kernels in the frequency domain, e.g., Bessel, Butterworth, Chebyshev using MATLAB's signal processing tool box) were tested. Finally, only very basic filtering was applied because in general filtering was not needed as the suddenly occurring bubble signals were well above the background noise. Furthermore, all filters change the signal and particularly have problems with reflecting sudden changes (the start or end of a bubble release event) truthfully. Thus the raw signal was processed as unchanged as possible.

[16] Spectrum analysis via FFT used the software code given by *Smith* [2002]. Data gaps caused by the chosen ping/sleep interval were ignored for band-pass filtering. As spectrum analyses were performed on stacked traces, data gaps were filled with zeros to get a continuous and equidistant data set. Zero padding was applied to get a data set of 2^n values. A maximum of 65,536 values (n = 16) for the FFT input data set was used to analyze the 34,400 pings (~45,900 samples if the time gaps are filled). Hann and Hamming windowing was tested and compared to rectangular windowing (= unchanged trace values). Although weak leakage could be observed with rectangular windowing, the spectra shown are processed with a rectangular window. This is because the bubble burst patterns are not strictly periodic but in some cases erratic or discontinuous. Applying Hann and Hamming windowing in some cases suppressed frequencies, which for nonwindowed analyses could be clearly seen and matched with bubble release events in the stacked raw data.

[17] To detect seeps in the data set and to visualize their activity, size and influence of currents on the rising bubbles, swath and trace plots were used. The final quantitative analyses for one seep were carried out on stacked traces that were cleaned for spikes using logical relations rather than mathematical filters. The detection of bubble release events/bubble bursts was based on defining the background level and setting a threshold above which the respective trace value is counted as bubble detection. Even with the simple filter algorithms used, bubble seeps could be well detected and studied for temporal variability.

3.2.1. Swath Plots

[18] Swath plots, gray shaded xyi (512 cells, 21 beams, intensity) images where used to identify areas of potential seep positions (Figure 4). Various i-values for each trace were gained from the processing. These are (1) the number of bubble release events, (2) the integrated intensity of these events (sum of $ftv - bg$ for all bubble release events), and (3) the total amplitude of each trace.

[19] Background levels for each individual trace were defined by convolving the data with a boxcar filter kernel of a time window of more than 500 trace values (pings; equation (3)) or the mode of the entire trace. The mode value was set to the smaller value for bimodal distributions.

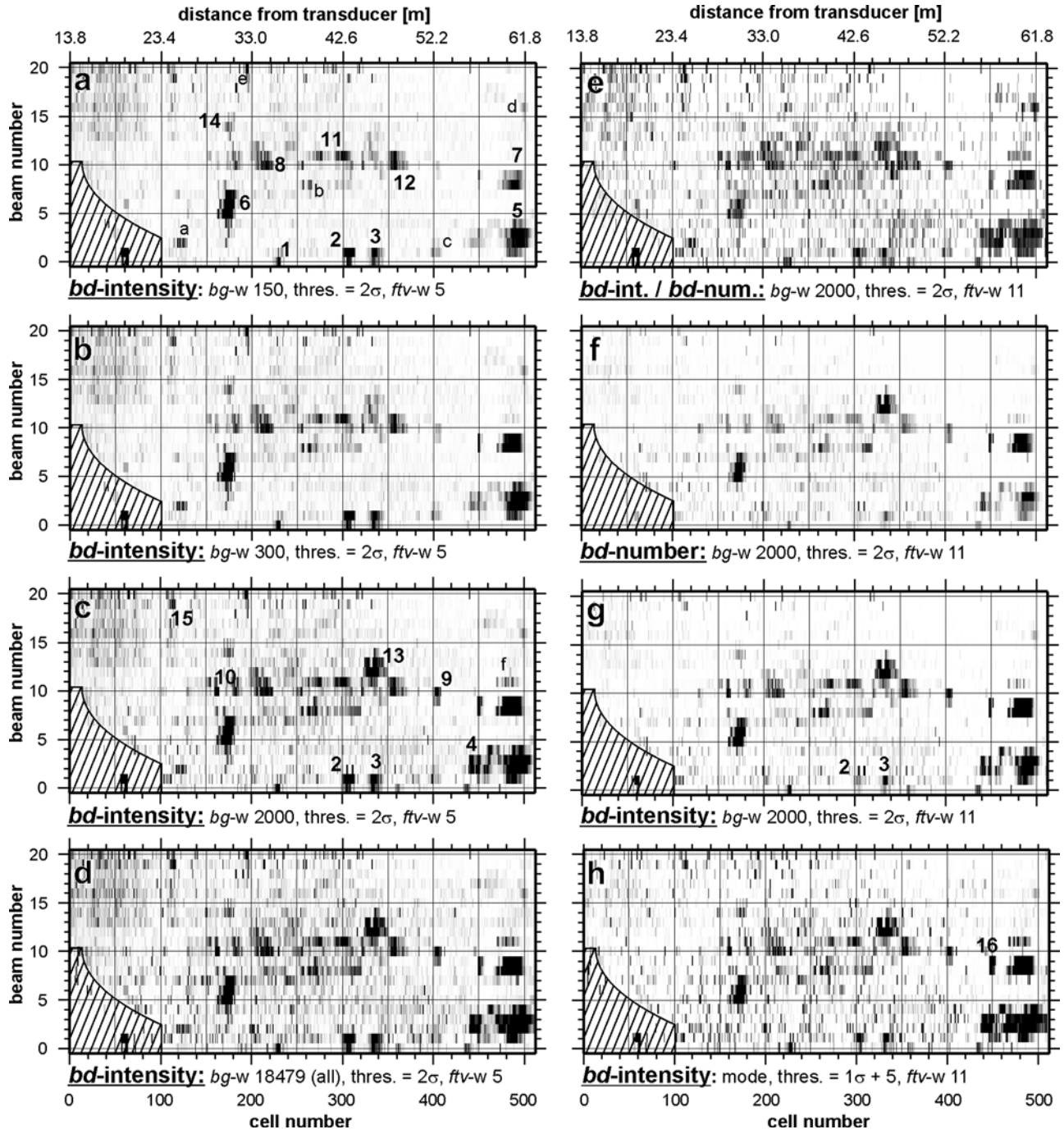

Figure 4. Swath plots, processed with different window widths for the background ($bg - w$) detection, smoothing of the trace ($ftv - w$) and thresholds for bubble release event detection. The data represent only the first half of the deployment. (a–d, g, h) Integrated intensity of all bubble detections events (*bd*). (f) Number of bubble detection events per trace. (e) Relative seep intensity *bd*-intensity/*bd*-number. Spots within panels labeled with letters a–f did not fulfill the criteria of a bubble site (see text).

The threshold level was defined by a static offset value and/or x times the standard deviation of all unfiltered trace values. Using the standard deviation was important for taking into account the different noise levels between traces. Noise was reduced applying a moving average of a short window (< = 11 pings, equation (2)). A trace value was identified to be caused by bubbles (bubble detection, *bd*) according to (1).

$$bd \text{ is given if } ftv > bg + x * \sigma + soff, \tag{1}$$

$$ftv_n = \frac{1}{(2w+1)} \sum_{n-wf}^{n+wf} rtv, \tag{2}$$

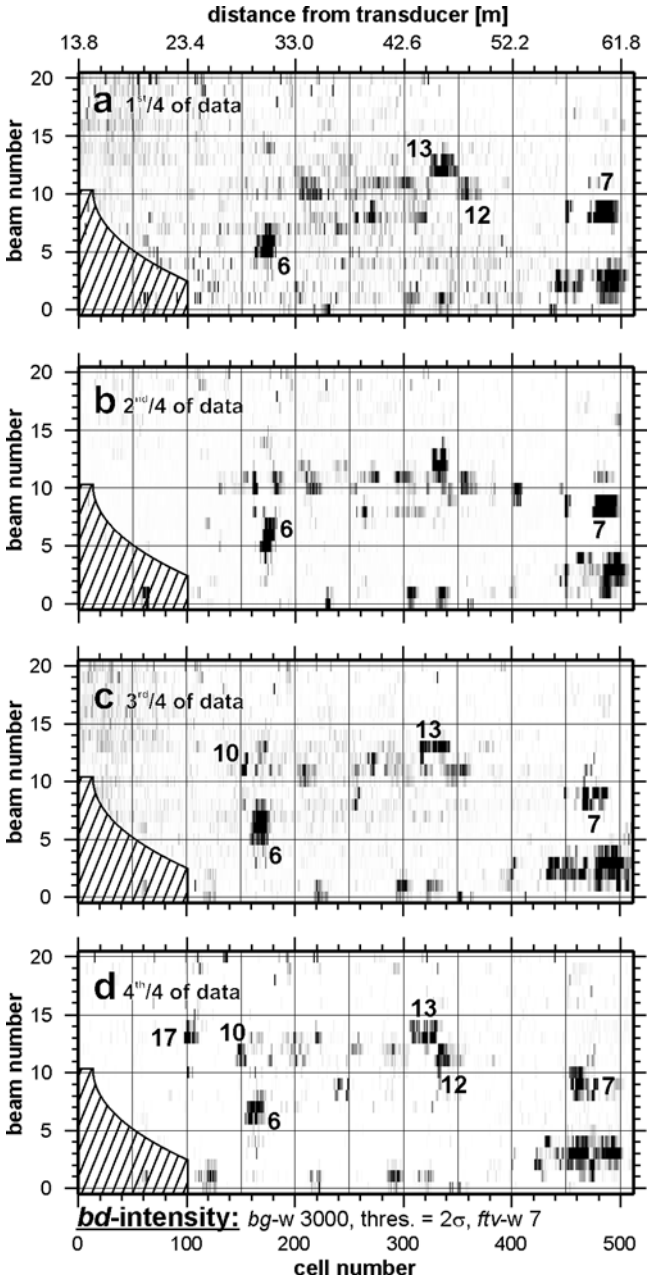

Figure 5. Swath plots depicting the entire data set divided into four equal time periods. The plots show the integrated intensity of bubble release events detected. The data were smoothed by a moving average of seven values (28 s); the threshold was set to 2σ. Changes in intensity and particularly in position (seeps 6, 10, 12, 13, 17) highlight the transient behavior of bubble release and the influence of currents, respectively.

$$bg_n = \frac{1}{(2w+1)} \sum_{n-wb}^{n+wb} rtv \text{ or mode value of these data,} \quad (3)$$

$$\sigma = \sqrt{n\_\max \sum_{1}^{n\_\max} rtv - \left(\sum_{1}^{n\_\max} rtv \right)^2 \Big/ n\_\max^2}, \quad (4)$$

with:

bd = bubble detection;
ftv = filtered trace value;
rtv = raw trace value;
bg = background value;
soff = static offset;
σ = standard deviation;
wf = half window width for filtering;
wb = half window width for background;
n = trace value number (ping number).

[20] Figures 4a–4d and 4h show the same raw data processed with different background settings and threshold levels. In all plots, the majority of the 17 detected seep sites can be easily seen; some seeps become visible more clearly at specific settings depending on their activity pattern.

[21] Seeps releasing short bubble bursts (<1 min) show up regardless of the background window width (>500) or the mode value defining the background (e.g., seeps 2, 3, 6 in Figure 4). Seeps with fewer but longer bubble release events need a larger window for background detection or the mode value to be identified. Setting the width of the filtering moving average window wider suppresses noise (compare Figures 4c and 4g) but also weakens very short bubble bursts in such a way that they are not recognized as bubble release events anymore (compare seeps 2 and 3 in Figures 4c and 4g). Dividing the integrated intensity of bubble detections in one trace (Figure 4g) by the number of bubble release events (Figure 4f) yields a relative intensity of a seep characterizing how 'vigorously' a seep is bubbling (Figure 4e).

[22] All swath plots in Figure 4 are based on the data of only the first half of the recorded time. In comparison, Figure 5 shows four swath plots, each of them displaying a quarter of the entire data set. Variations in strength (e.g., seep 6) and a shifting of the seep position toward the transducer with time (e.g., seeps 7, 10, 12, 13) or shifting between beams (seep 6) becomes visible. Seep 17 appears exclusively in the plot of the last quarter as it was only active for the last 46 min of the deployment.

3.2.2. Trace Plots

[23] The bubble release activity and the shifting of bubbles in the swath plane can be seen in more detail in trace plots, where a series of traces is plotted above each other. As an example, seep 6 is shown in Figure 6. Intensity differences within traces clearly show where and when bubbles crossed the swath plane. Owing to the strong backscattering of bubbles, backscattered signals are also detected by the side lobes of neighboring beams or outside the nominal ~3 dB beam angle width and cause higher intensities within respective traces. Owing to the oversampling (1 ms pulse length, 128 ms sampling interval), similar patterns can be seen in 5 or more consecutive traces. The sinusoidal shift of the high intensities toward and away from the transducers (changing cell numbers) is caused by water currents that move the bubbles in the swath plane 3 m above the bottom horizontally from their origin at the seafloor. Points A and B (beam 7) in Figure 6 mark two centers of the bubbles 1.4 m apart at two different times. Assuming a rather fast bubble rising speed of 30 cm/s, bubbles need 10 s to rise 3 m into the swath plane. Currents of 14 cm/s are needed to shift the bubbles by 1.4 m, which is in good

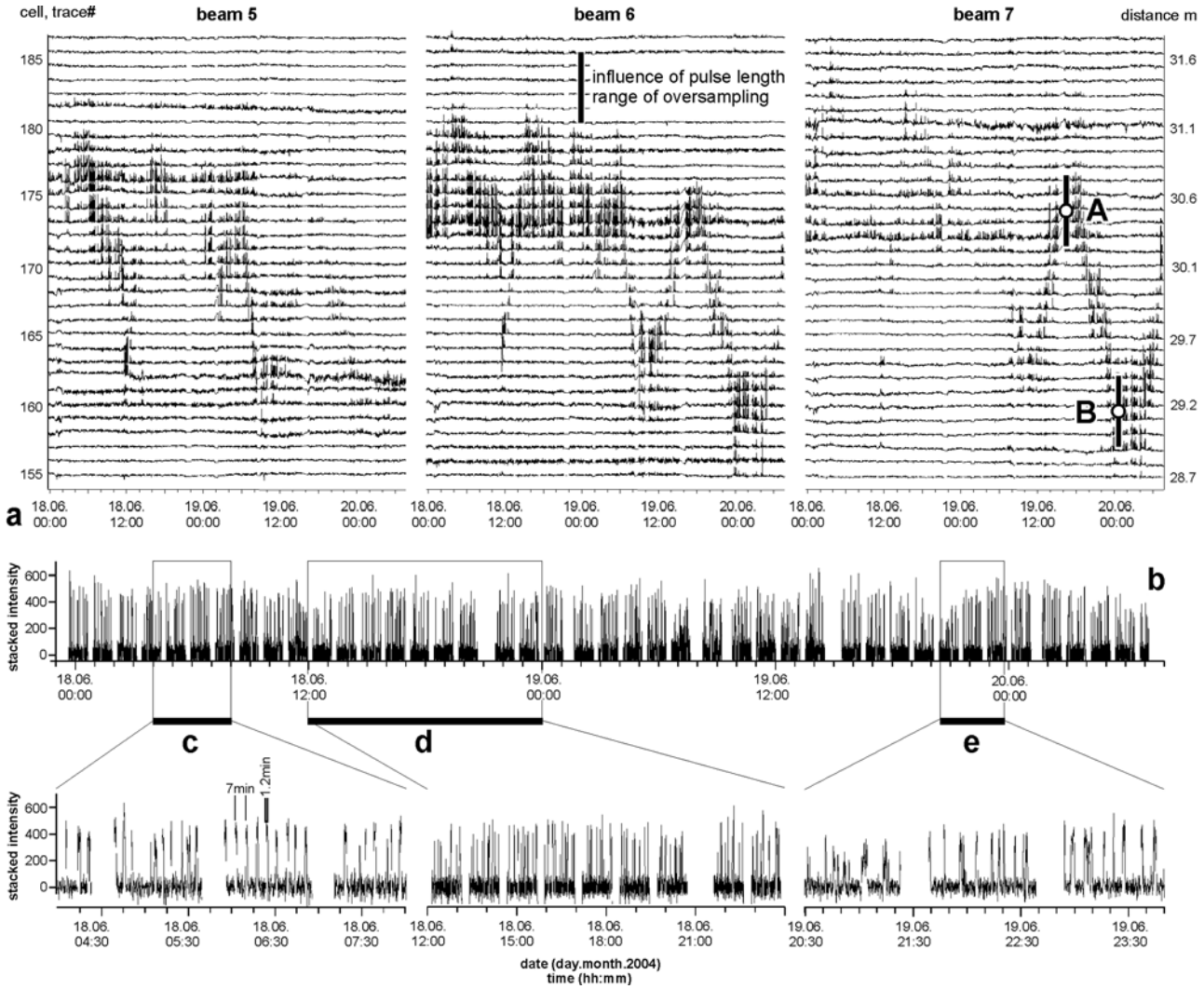

Figure 6. Trace plot showing data from the frequently active seep 6. (a) Traces (amplitude changes over time) of three neighboring beams (5–7) for samples 155 to 187 (28.7 to 31.8 m distance from the transducer). Owing to the 1-ms pulse length but 128-ms sampling interval of the received signal, very similar patterns can be seen in six consecutive traces. Taking this into account, points A and B in beam 7 mark the center of the bubbles crossing the swath plane 1.4 m apart at two different times. Assuming a bubble rising speed of 30 cm/s, bubbles need 10 s to rise into the swath plane 3 m above the bottom. Currents of 14 cm/s are needed to shift the bubbles by 1.4 m, which is in good agreement with the current velocities shown in Figure 2. (b) Stacked raw data of all traces from beams 5 to 7 representing the overall release activity of this particular seep. (c–e) Enlarged time intervals as indicated in Figure 6b. All *x* axes represent date (in 2004) and time (hh:mm); *y* axes in Figures 6b–6e represent the stacked amplitude intensity.

agreement with measured current velocities as shown in Figure 2. Thus water current changes are most likely the reason for the shift of the bubble position in the swath plane rather than different bubble releasing holes in the seafloor. Very similar shift patterns have been observed for other frequently active seeps such as 4 or 1, confirming this assumption (Figure 13 and Figure S1 in the auxiliary material[1]).

[24] Because of these shifts it is important to combine all traces that belong to one seeping hole for getting the overall seep activity. This was done by stacking (simple adding) all traces showing indications of bubble release, followed by smoothing and system drift corrections by band pass filtering, moving averages, polynomial regressions or manual background picking. Figure 6b shows stacked raw data from beam 5 to 7 representing the overall release activity of this particular seep. Figures 6c–6e show three time intervals enlarged that clearly show the temporal variability of seep 6. Comparing beam 5 and beam 7 reveals that currents do not only move the bubbles to and away from the transducer, but also left and right. At the beginning of the data set, higher intensities can be seen in beam 5 which became very weak in the second half of the deployment. As a result, bubble

[1]Auxiliary materials are available in the HTML. doi:10.1029/2007JC004704.

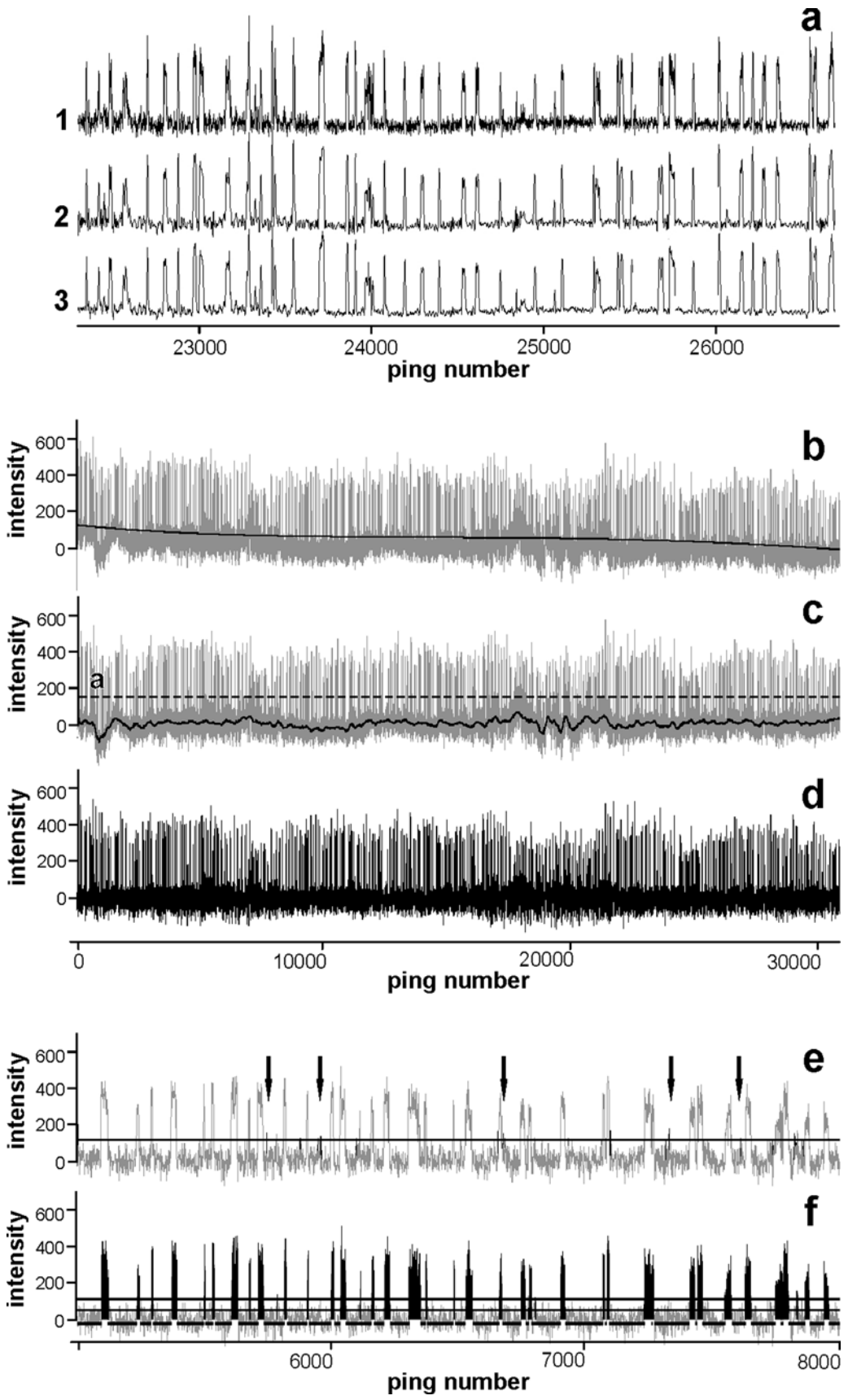
a
1
2
3
23000
24000
25000
26000
ping number
b
intensity
600
400
200
0
c
a
d
0
10000
20000
30000
e
f
6000
7000
8000

Figure 7

release events became much stronger in beam 7 during the second half (see also swath plot in Figures 5a and 5d).

3.2.3. Final Bubble Seep Identification

[25] The final decision if high amplitudes in swath or trace plots are caused by bubbles released from seeps was based on a few simple criteria. Bubble release from one seep will not be permanent over a longer time (>1 day) in most cases, thus the amplitude values in one trace will change over time. Owing to currents bubbles are shifted from one cell to another and will not be recognized permanently in one cell/trace. Again, amplitude values over time will change in one trace. Because of the oversampling of data, using a 1 ms pulse but a 128 μs sampling rate, similar backscattered signals from bubbles (or other targets) should appear in 5–8 consecutive traces (Figure 6). Bubble release events seen during the JAGO dive in the Black Sea and also elsewhere typically start and stop rather suddenly. Thus intensity changes in traces caused by bubbles will have a rectangular shape.

[26] Misidentifying fish as bubbles is a general problem, but two additional criteria were used to prevent such misidentification. It is unlikely that fish stay 3 m above the bottom at one spot for a longer time (>5 min) without any signs of movement despite currents. Thus strong intensity changes that occur only once in a trace but last for longer were counted as bubble detection. In 92 m water depth in the Black Sea the water is already strongly reduced in oxygen and the number of fish is extremely low (only occasionally small fish were seen at the bottom, never in the water column). Using these criteria, 17 seep sites were identified in the data set, all showing specific activity patterns.

3.2.4. Seep Activity Analyses

[27] Studying the activity patterns of bubbling seeps provides insights into the internal and external forces that trigger and modulate the bubble flux. The activity of single seeps as well as of the entire seep area can be studied by looking at: (1) the activity as a percentage of the time measured (relative activity); (2) the integrated strength of the bubble release events; (3) the distribution of the different lengths of the active and inactive periods (i.e., mean, median or mode length); or (4) the correlation between bubble release event lengths and their integrated strength. Comparing the activity of two or more seeps located close to each other might reveal similar activity patterns that indicate a joint gas reservoir fuelling both seeps. Furthermore, describing the changes of the number of seeps active in the entire area at one time or their integrated strength might provide insights into the variability of gas flux from deeper sediment horizons, or the impact of tides/currents on the fluid system causing the entire area to 'breathe.'

[28] The activity pattern of one seep can be analyzed either by stacking (raw) traces first and performing the activity analysis afterward with this combined data set, or by first analyzing the activity trace by trace and then combining the results. Stacking data first has the advantage of increasing the signal-to-noise ratio, mainly by the fact that 4 to 6 consecutive traces will have very similar patterns. This advantage turns into a disadvantage with very active to permanently active seeps, where stacking results in a rather constant, elevated intensity level without a clearly identified background.

[29] Filtering that reduces low-frequency changes of the background (e.g., due to a oscillating amount of particles in the water) and high-frequency noise in stacked data has been performed by band-pass filtering, moving averages of different window size (equations (2) and (3)), polynomial regressions, as well as visual background digitizing or combinations of these methods. For all activity analyses presented here stacked raw data traces were used. Low-frequency background level fluctuations and trend-like changes were corrected by using polynomial regressions (Figure 7b), and calculating a moving average (window of 50 to 200 samples) but excluding data above a certain threshold (line a in Figure 7c) and replacing this value with the mean of the entire trace. This threshold as well as the threshold above which a trace value is counted as bubble detection was defined by the 1σ or 2σ level of the stacked trace values but in some cases was visually adjusted just above the background noise level. In addition, trace values were seen as spikes if the two previous and two following trace values were below the bubble detection threshold of 1 or 2σ. Those values were set to the corresponding background level (Figure 7e).

[30] Bubble release events for the final activity analysis were defined by applying a logical relation similar to a Schmitt trigger in electronics. A band of uncertainty is defined by two intensity levels (here: upper level = threshold, lower level = threshold/2) and all values above the upper level are counted as bubble detection. Adjacent values (toward higher and lower ping numbers), which are below the upper but above the lower level, are also counted as bubble detection until the value drops below the lower limit (Figure 7f).

[31] Stacking data first and defining the background level afterward might cause problems with very active seeps where only a few values define the actual background. Low-frequency variations might be linked to higher amounts of suspended material in the water column or system drift. Erroneously correcting these variations will have a tremendous impact on the final activity calculations. However, in some individual stacked traces the background can be defined quite easily but very active seeps might have to be processed in several steps or by adding trace by trace in an iterative processes involving background correction while doing so (this was done for seep 4 and 5).

Figure 7. (a) Visualization of processing steps and comparison of raw (line 1), low-pass-filtered (line 2) and moving average-smoothed data (line 3). Both filter methods (lines 2 and 3) provide very similar results. Processing starts with background/drift correction by applying (b) polynomial regression and (c) moving averages shown as black lines. (d) Data used for the activity analysis of seep 6 after the processing steps shown in Figures 7b and 7c. After the background correction, spikes are removed (see text for more explanation). (e) Black data are spikes, and the horizontal line is the threshold (here 1σ; only a subset of the data is shown). (f) Final bubble release event detection applying the Schmitt-Trigger method; bubble events and the inactive periods are shown in black.

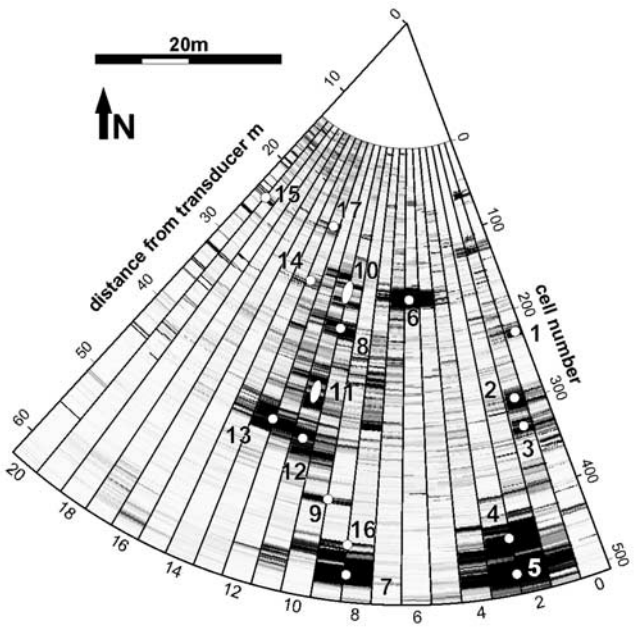

Figure 8. Location of the 17 seep sites in the hydroacoustic swat shown as gray-shaded swath plot for the intensity of all data processed. The seeps clearly show up with their real distance to each other.

[32] The amount of active and inactive periods, their lengths and the integrated strength of bubble release events can be used to describe the activity of the different seeps and the entire seep area.

4. Results

4.1. Activity Variations of Single Seeps

[33] All in all, 17 bubbling seeps have been identified (Figure 8) within the 38 h 13 min period of data recording during the 55 h 22 min deployment (Table 1). On the basis of their activity patterns, seeps could be classified into three major groups: (1) sporadically active, in irregular bursts between 8 s and <20 min length with sometimes more than 10 h of silence (<200 bursts, active time < = 5%); (2) regularly active, in bursts of 8 s to 22 min throughout the entire observation time with sometimes periodic releases, inactive periods are not longer than 3 h (200–350 bursts, active time 5 to 20%); or (3) frequently active, in bursts typically not longer than 3 min with a sometimes regular periodicity (>350 bursts) or seeps which are active for more than 20% (Figure 9) showing single bursts of up to 1 h 16 min. In the following, examples are given for the different release patterns.

4.1.1. Sporadically Active Seeps

[34] Sporadically active seeps (6 of 17) were not active during most of the observation time and only on very few occasions showed some kind of periodicity. Seep 9 is an example for a single but rather long bubble burst followed by a few shorter ones, which are significantly weaker (Figure 10). As another example, the area of seep 10 is more active with a few short bursts occurring irregularly 30 to 32.5 m away from the transducer (Figure 11a). Three ~10-min-long bursts can be seen in traces 145–170 (27.7 to 30 m from the transducer). As they are separated from the previous ones between samples 175 to 195, they actually represent another seep within the 4 m distance covered. These three longer bursts occur regularly every 18.5 h with no other significant activity visible in the meantime. Similar to seep 6, bubbles were current-drifted parallel to the transducer face with strong amplitudes in beam 10 for the first burst (weak in beam 12) but strong amplitudes in beam 12 for the third burst (Figure 11a).

4.1.2. Regularly Active Seeps

[35] Regularly active seeps (6 of 17) either show a few long bursts as in seep 13 (Figure 12) or many short bursts as in seep 14 (Table 1). It seems long bursts occur with

Table 1. Position, Time, and Type of Activity of the 17 Bubbling Seeps[a]

Seep	Position Beams/Cells	Number[b]	Total[c]	Burst Length, Pause Length				Active
				Longest	Mean	Median	Mode	
1	0–1/ 205–240	182	0:57:20 2.5%	0:01:40, 1:20:52	00:19, 12:17	00:14, 04:12	00:08, 00:04	sporadically
8	10–11/ 195–225	149	1:16:48 3.4%	0:04:00, 1:41:24	00:31, 14:53	00:21, 06:25	00:21, 00:04	
9	9–10/ 395–415	14	0:22:24 1.0%	0:18:00, 13:01:20	0:01:36, 2:42:12	00:22, 09:44	00:16, 00:52	
10	10–12/ 165–195	155	1:40:00 4.4%	0:10:28, 3:59:36	00:39, 14:09	00:18, 01:02	00:12, 00:04	
12	10–11/ 330–375	134	1:29:40 3.91%	0:03:24, 1:50:32	00:40, 16:27	00:31, 05:40	00:12, 00:04	
17	13/ 95–115	40	0:19:28 0.9%	0:04:40, 10:37:36	00:29, 56:51	00:10, 04:16	00:08, 00:04	
3	0–1/ 320–350	292	2:00:16 5.2%	0:03:08, 1:26:08	00:25, 07:26	00:18, 03:46	00:20, 00:04	regularly
7	8–9/ 460–500	82	2:57:24 7.7%	0:12:32, 2:06:58	02:10, 25:48	00:58, 07:00	00:20, 00:04	
11	10–12/ 265–315	218	1:39:40 4.4%	0:08:00, 1:27:16	00:27, 10:04	00:18, 02:40	00:16, 00:04	
13	12–14/ 315–355	194	3:58:16 10.4%	0:22:16, 3:02:20	01:14, 10:36	00:19, 00:19	00:08, 00:04	
14	14/ 165–190	303	1:03:12 2.8%	0:02:24, 2:04:52	00:13, 07:22	00:07, 01:43	00:04, 00:04	
16	8–9/ 445–460	109	02:47:08 7.3%	0:12:32, 1:49:20	01:32, 19:30	00:38, 05:30	00:16, 00:04	
2	0–1/ 285–315	409	2:21:16 6.16	0:01:20, 0:25:36	00:21, 05:15	00:17, 04:30	00:16, 00:04	frequently
4	1–3/ 421–478	615	28:54:20 75.6%	1:16:12, 0:15:00	02:49, 00:55	00:55, 00:21	00:12, 00:04	
5	1–4/ 480–512	677	17:22:48 45.5%	0:23:48, 0:31:40	01:32, 01:51	00:55, 00:52	00:24, 00:04	
6	5–7/ 155–185	511	6:53:44 18.0%	0:03:48, 0:15:04	00:49, 03:40	00:40, 03:16	00:32, 03:16	
15	19–20/ 105–120	594	1:41:08 4.4%	0:02:00, 8:56:32	00:10, 03:41	00:06, 00:18	00:04, 00:04	
All			77:44:52					total

[a]Sporadically active: seep 5 to 17; regularly active: seep 3 to 16; frequently active: seep 2 to 15. Notation: h:mm:ss or mm:ss. Deployment information: start of pinging, 17.06.2004 at 23:42; stop of pinging, 20.06.2004 at 07:04; time at the seafloor, 55:22:00; total time of pinging, 38:13:20 (69%). Seep activity information: integrated time all seeps have been active, 77:44:52; averaged active time for one seep, 04:34:24 (11.9%).

[b]Number of bubble bursts.

[c]Active time and percentage of total time.

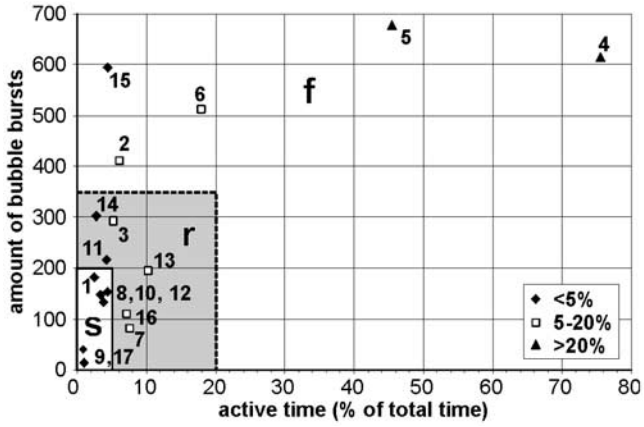

Figure 9. Plot used to classify all seeps into three groups, sporadically (s), regularly (r), and frequently (f). Black diamonds are seeps active for less than 5% of the time; open squares are active between 5 and 20% of the time; black triangles are active for more than 20% of the time. Numbers represent the seep number.

some regularity and do not cluster at a point in time. Although it was found that the bubble release occurs either in short or long bursts, seep 7 shows a quite distinct bimodal distribution around 30 s and 4.5 min long active periods (Figure 15).

4.1.3. Frequently Active Seeps

[36] Five frequently active seeps were identified (e.g., seep 6, Figure 6), but only one seep was bubbling for more than half of the time (seep 4, 75% active; Figure 13) and one other was active for more than 20% (seep 5, 45%; Table 1). All other seeps release bubbles for less than 20%, whereas seep 6 is quite active with sometimes very periodic bursts that are on average 49 s long (Table 1). In contrast, seep 15 shows the third highest number of bubble release events but is only active for less than 5%. Owing to the great number of short bursts it was classified as frequently active and it is a good example for the many different bubble release patterns.

4.1.4. Temporal Variability of Single Seeps

[37] Spectral analyses for seep 6 show a dominating frequency of 3.2 min and 5.9 min for one short period with a very regular bubble release pattern (Figure 14); 5.9 min very nicely represents the longer burst intervals of about 1.2 min, whereas the 3.2 min frequency mainly fits with much shorter bursts of around 30 s. The 3.2 min frequency remains dominant for the complete data set with three other strong frequencies at 4.23, 5.39 and 11.6 min. No lower frequency appeared that might indicate a tidal relation of bubble release. The two stronger frequency bands at 72 and 35 min are related to the chosen ping setting (~1 h pinging, 15 min pause).

[38] Power spectra for three more seeps are displayed in Figure S2 in the auxiliary material, one for each type of activity. Seep 2 is frequently active and shows few dominating frequencies between 12.4 and 3.4 min. At 6 min, a spike stands out in the spectrum representing the periodicity of 30- to 40-s-long bubble burst. The sporadically active seep 8 does not have a particular frequency but a few that stand out a little with frequencies between 21 and 5 min. The nonexistence of one dominant frequency for the 149 detected bubble release events indicates that this seep is erratically active. The bimodal, regularly active seep 7 does not show a dominating frequency for its 82 release events.

[39] In addition to power spectra, the activity patterns were visualized by plotting the distribution of active and inactive periods as sum curves (Figure 15). It was found that by far short bubble bursts of less than a minute dominate the bubble release of all seeps. Except for four seeps, more than 90% of all bubble release events are shorter than 2 min. Not even the two most active seeps (4 and 5) show a median value for the burst length of one minute (55 s for both, Table 1). A strong bimodal distribution becomes visible for seep 7 (~30 s and ~4.5 min) and 4.5-min-long active periods also occur more often at seep 16. As the data were not filtered at all, short inactive periods of 4 s are very common. Only at the two least active seeps inactive periods are longer than 2 h, which indicates that the activity in general occurs on a 'regular' basis and not clustered around a certain time with longer inactive periods as one would assume for a strongly tide-dependent bubble release.

4.2. Activity Variations of the Seep Area

[40] The integrative activity of all 17 seeps was analyzed by counting the number of seeps active at the same time, and by adding the stacked intensity values of all seeps at the time they were identified as active. A maximum of 9 simultaneously bubbling seeps was found with two clusters of more than 7 seeps being active 18 h after another (Figure 16a). More than three seeps were only active for less than 20% of the time. Most often, three seeps were bubbling simultaneously (37%) and the entire area was inactive during 10% of the time.

[41] Plotting the stacked intensity of all bubble releasing vents over time (including the two most active seeps 4 and 5) shows an increase and decrease that correlates only occasionally to the number of simultaneously active seeps (Figure 16b). Spike-like high values typically coincide with high numbers of simultaneously active seeps, although this is not true at 0700 local time on 19 June 2004. The general decrease in stacked intensity coincides with a drop from on average three to only two simultaneously active seeps toward the end of the data set.

[42] Spectrum analyses for the amount of simultaneously active seeps did not show any dominating frequency that might indicate some kind of periodicity. In contrast, the stacked intensity shows two dominating frequency bands in the power spectrum around 728 min and 124 min (Figure 16c). The longer period describes a pulsing that is equivalent to that of the almost permanently active seep 4. Without seep 4 and 5, no periodicity is visible at all and variations of the stacked intensities are very similar to those of the number of active seeps. The shorter period of around 124 min is certainly strongly influenced by the chosen ping/pause interval.

5. Discussion

5.1. Temporal Variability of Bubble Release

[43] The discovered variability and periodicity in bubble release was not really unexpected. Periodic fluid release on very different timescales is known from many seeping or

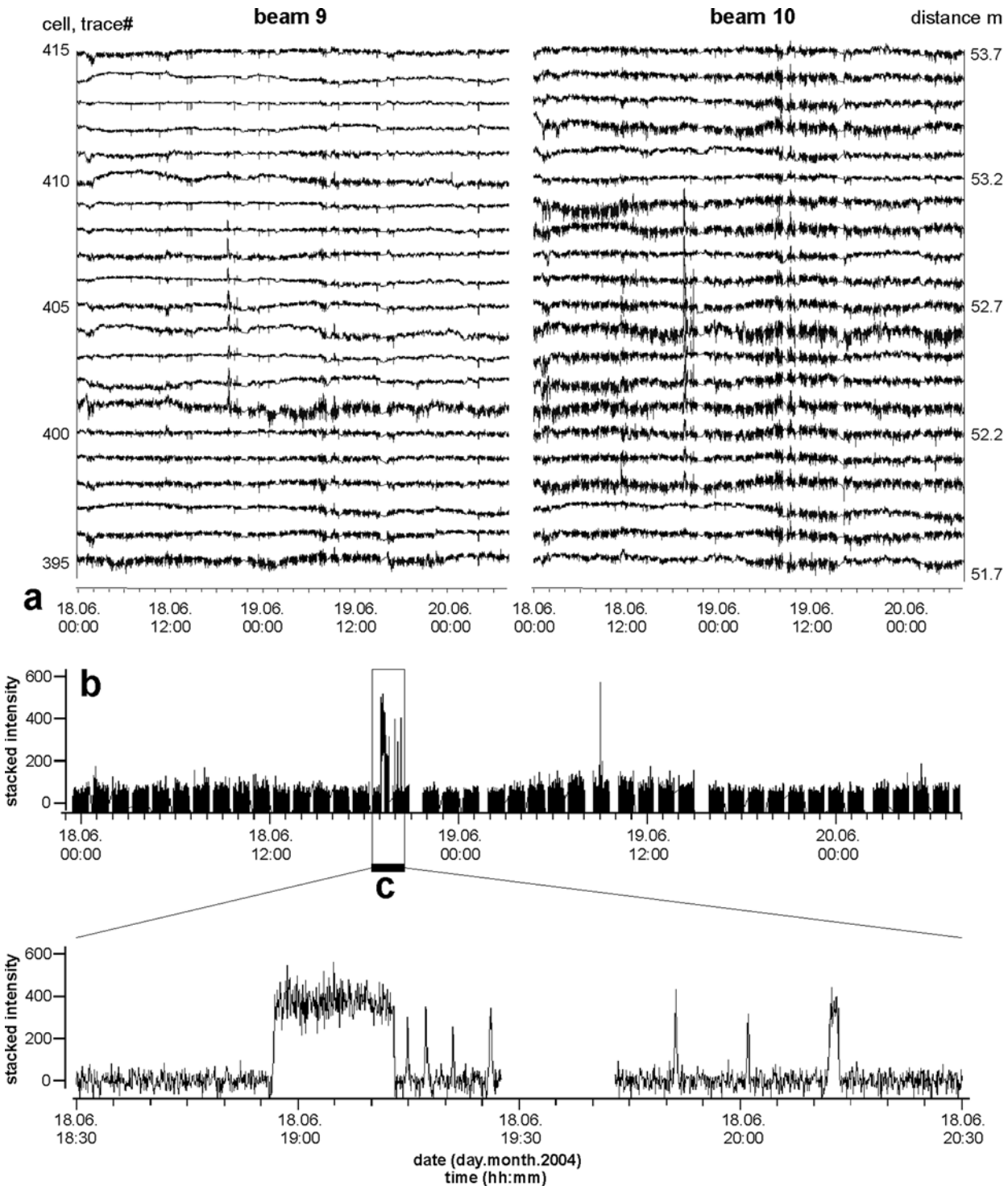

Figure 10. (a) Trace plots of the sporadically active seep 9 detected in beams 9 and 10. (b, c) Only one long burst (18 min) was detected in the stacked data, followed by four shorter and weaker bursts in the following 1.5 h. Only very few short and weak bursts occurred after this single main event.

venting systems like hydrothermal geysers or mud pools. Tide-dependent bubble release from cold seeps has been described for Hydrate Ridge [e.g., *Heeschen et al.*, 2003]. Short-term fluctuations have to be assumed for seeps which are reported to have a 'pulsing' bubble release [*Leifer and MacDonald*, 2003; *Sauter et al.*, 2006]. In principle, the presented GasQuant data do not show release behaviors that have not been observed before, but they prove in a very high temporal and spatial resolution that individual seeps behave differently on all possible timescales within a distinct seep area.

[44] The main reason for the short-term variations observed by GasQuant (minutes to hours) is the capturing of free gas in a small reservoir close to the sediment/water

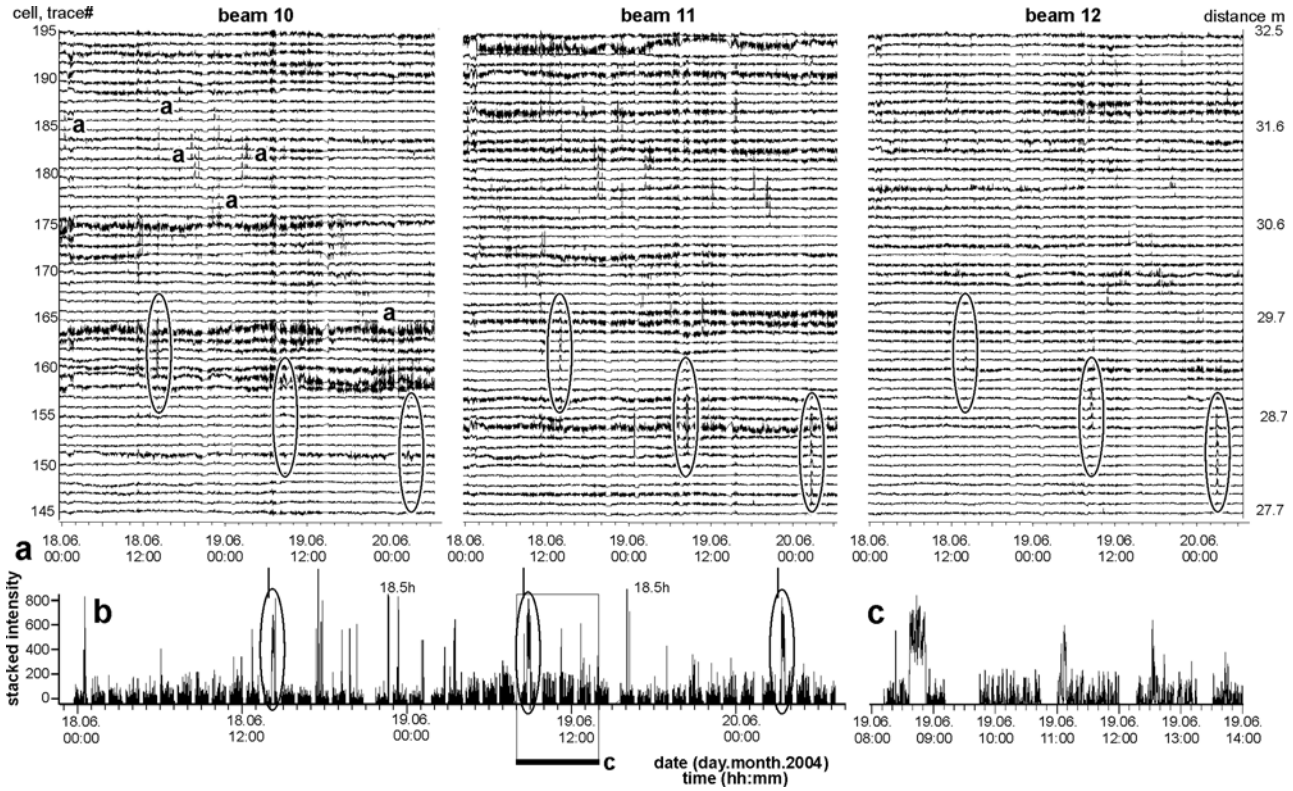

Figure 11. (a) Sporadically active seep 10 with few short and nonperiodic bubble release episodes. For visual purposes, traces of beams 10 to 12 are smoothed by a moving average of 11 pings. Three longer bursts are released from a second seep closer to the transducer (ellipsoids); they occur 18.5 h after each other and last for up to 11 min in stacked raw data traces. (b, c) Moving average-filtered data. Some samples are quite noisy and show strong background drift (e.g., beam 10: 164, 174; beam 11: 194); these traces were excluded for activity analyses.

interface until the pressure building up overcomes the trapping forces. During submersible dives, bubbles were seen to be trapped, for example, under bacteria mats or AOM-derived carbonate slabs just below the sediment surface [*Naudts et al.*, 2008].

[45] A constant supply of gas and unchanging physical parameters of the reservoir and its outlet are important for a periodic bubble release at those seeps. In natural environments it is unlikely that such constant conditions last for long and even the few time intervals in seep 6 that show a quite dominant periodicity (e.g., 5.9 or 3.2 min; Figure 14) still vary by few tens of seconds and do not last longer than an hour. The main reasons for this in general are that the gas supply and pressure conditions vary over time, for example, owing to tides (although this is not applicable in the Black Sea), and that shape modifications of the bubble releasing hole by currents, bioturbation, or mineral precipitation constantly alter the properties of the seep.

[46] In contrast to the single seep variability, the integrated activity of a seep area will be influenced to a higher degree by the gas supply and the internal cyclicity of the seep system fed by deep-derived fluids or material turnover in the surface-near sediments. In pressure-modulated seep areas, the number of simultaneously active seeps and the integrated strength will probably mirror this dependency but it might not be visible at one particular seep.

[47] The data show that none of the 17 seeps detected is continuously active and that the longest burst of 'only' 1 h and 16 min of the most active seep (seep 4, Table 1) does not immediately point to a seep that was active for 75% of the time it was observed. In average, each seep was active just for 12% of the time. Without the two most active seeps, this value drops down to 5.5%, which is quite low for an area that was classified as 'highly active' on the basis of hydroacoustic flare imaging surveys and visual observations of the seafloor [*Naudts et al.*, 2008].

5.2. Implications for Flux Extrapolations

[48] Because of these natural fluctuations, extreme caution must be applied if short-term direct flux measurements (although very accurate) are used for long-term flux estimates. Even direct measurements for tens of minutes or a few hours might not result in accurate free gas flux extrapolations. Assuming that the relatively long and vigorous burst of seep 9 (18 min) is a continuous process would tremendously overestimate the free gas flux at this particular seep. On the other hand, carrying out measurements at seep 4 during a period with only a few short bubble release events will strongly underestimate the flux at this seep. Thus long-term monitoring over at least one tidal cycle is essential to adjust directly measured fluxes to a mean flux that, to the best of the data-provided knowledge,

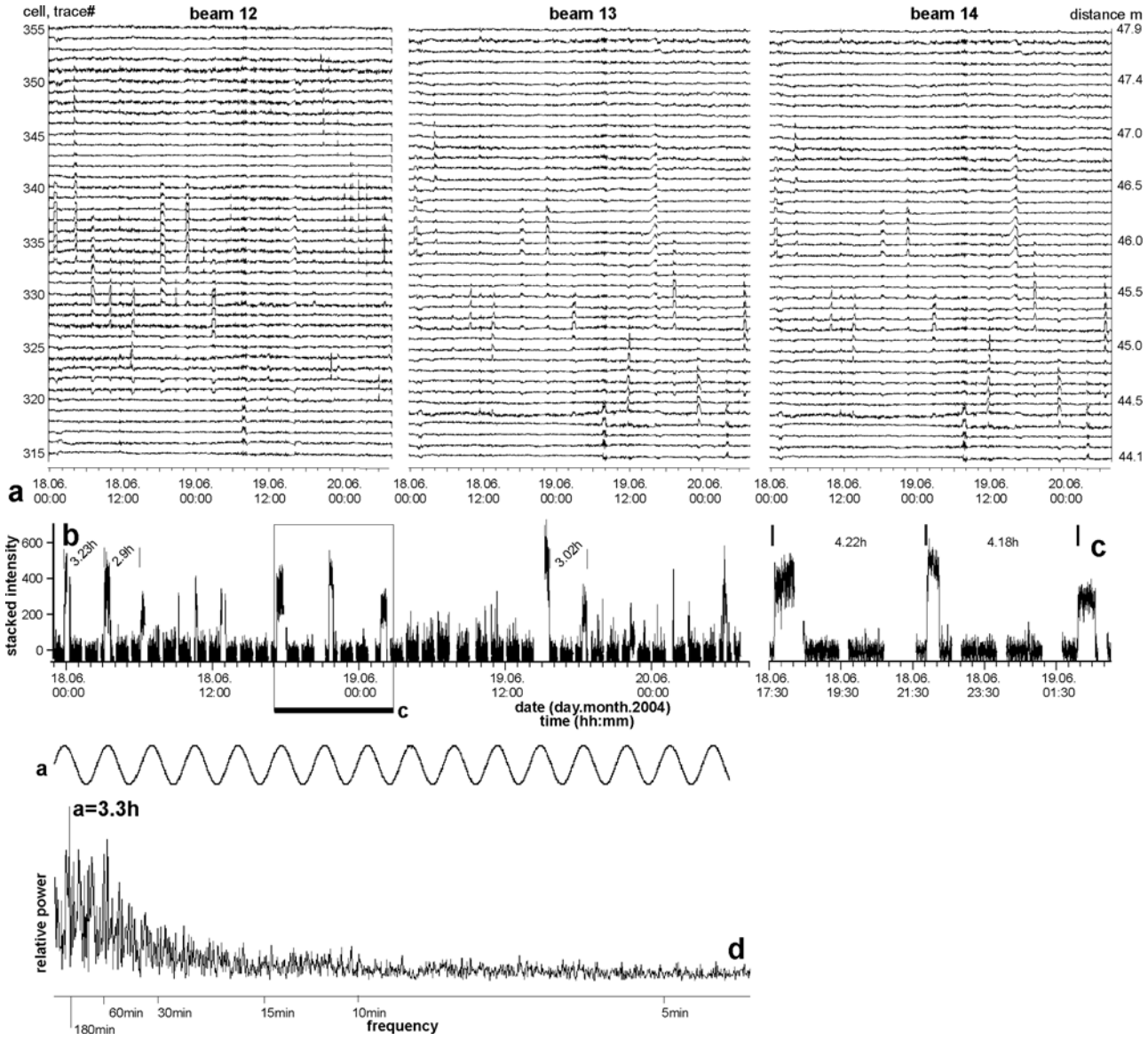

Figure 12. Regularly active seep 13 with few long bursts. (a) Traces were averaged over 11 pings. (b, c) Stacked raw data; the three bursts in Figure 12c are 29 (at least), 19, and 26 min long. (d) The power spectrum (no windowing applied) shows one dominant frequency at 3.3 h (letter a), which shows a reasonable fit to most of the bubble release events (sinusoidal line a).

is hopefully closer to reality. The accuracy in time and space should be high enough to resolve and detect even short bubble bursts. On the basis of the data presented, a 1 min resolution would be not good enough. To reliably detect a bubble release event, several (at least 5) successive pings should be sent within the overall mean bubble burst length, or as it is the case for the 4 s ping rate of GasQaunt, each bubble will be insonified at least once during its way through the horizontal swath.

6. Summary and Conclusions

[49] During a 55-hour-long deployment, the hydroacoustic swath system GasQuant simultaneously monitored the bubble release from 17 seeps at an area west of the Crimea Peninsula in the Black Sea in 92 m water depth. The received signal of each of the 21 beams is digitally stored in 512 samples (= 10,752 cells) between 14 and 63 m away from the transducer covering an area of about 2075 m^2. With a ping rate of 4 s (34,400 pings were sent in total; 38 h 13 min) and a cell depth of little less than 10 cm, GasQuant data sets provide high resolution in space and time.

[50] Very different release patterns could be observed and were categorized as sporadically, regularly and frequently active. Sporadically active seeps showed short bursts of less than a minute or a few bursts up to 20 min long (<200 bubble release events and active time < = 5%; 6 of 17). Regular active seeps showed bubble release events of less than a minute to a few minutes length throughout the entire time of observation; periodic release could be observed (200–350 bursts and active time 5 to 20%; 6 of 17). Frequently active seeps (5 of 17) either showed many short

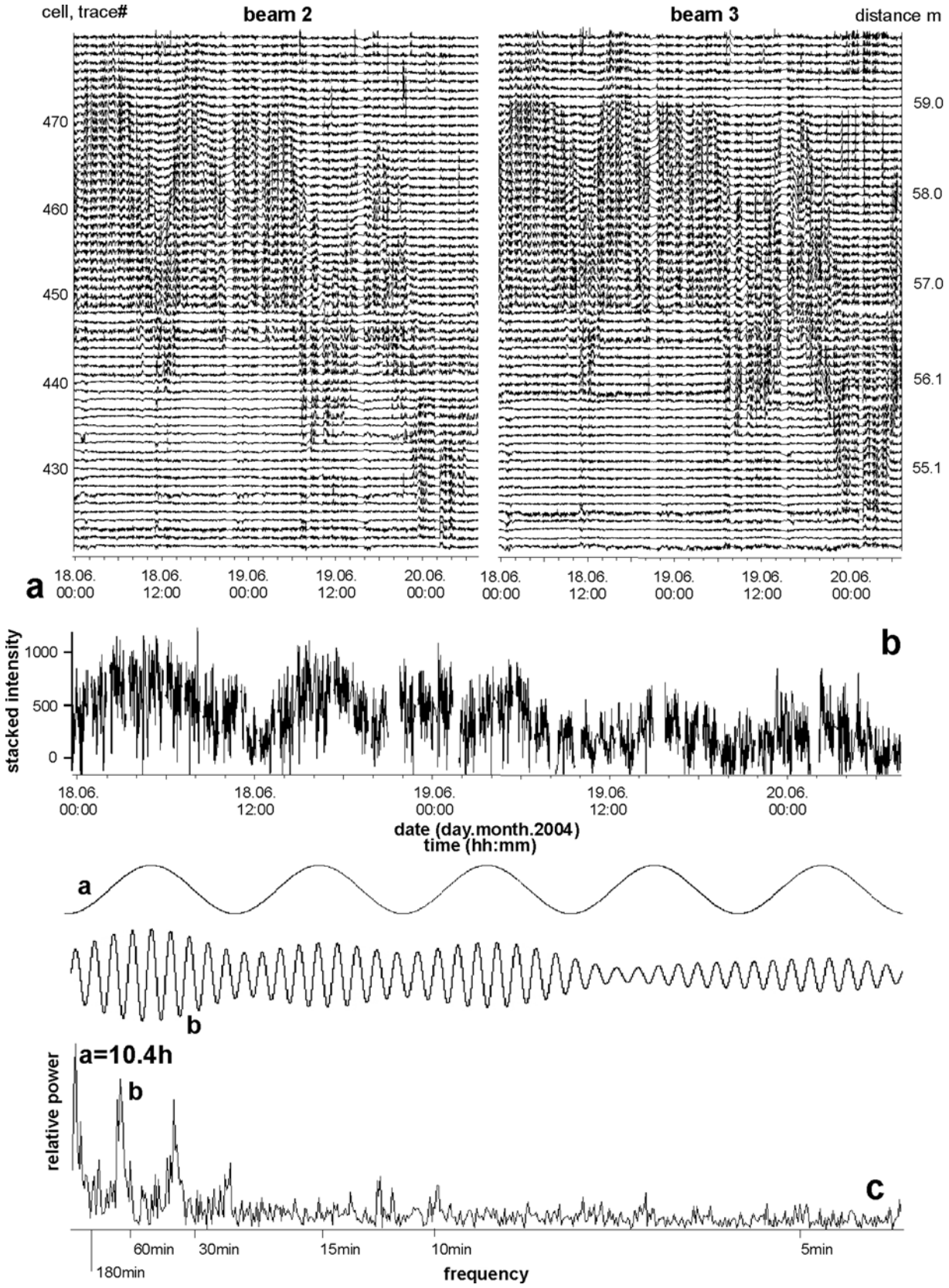

Figure 13. The most active seep 4 can be clearly seen in beams 2 and 3 in 58 m distance from the transducer. The power spectrum in C (no windowing applied) shows a strong frequency at point a (10.4 h) and frequencies clustered around point b (78 to 68 min), which are caused by the chosen system settings of 1 h pinging and 15 min pause. The up and down of the signal related to frequency a in this case is related to seep activity variations.

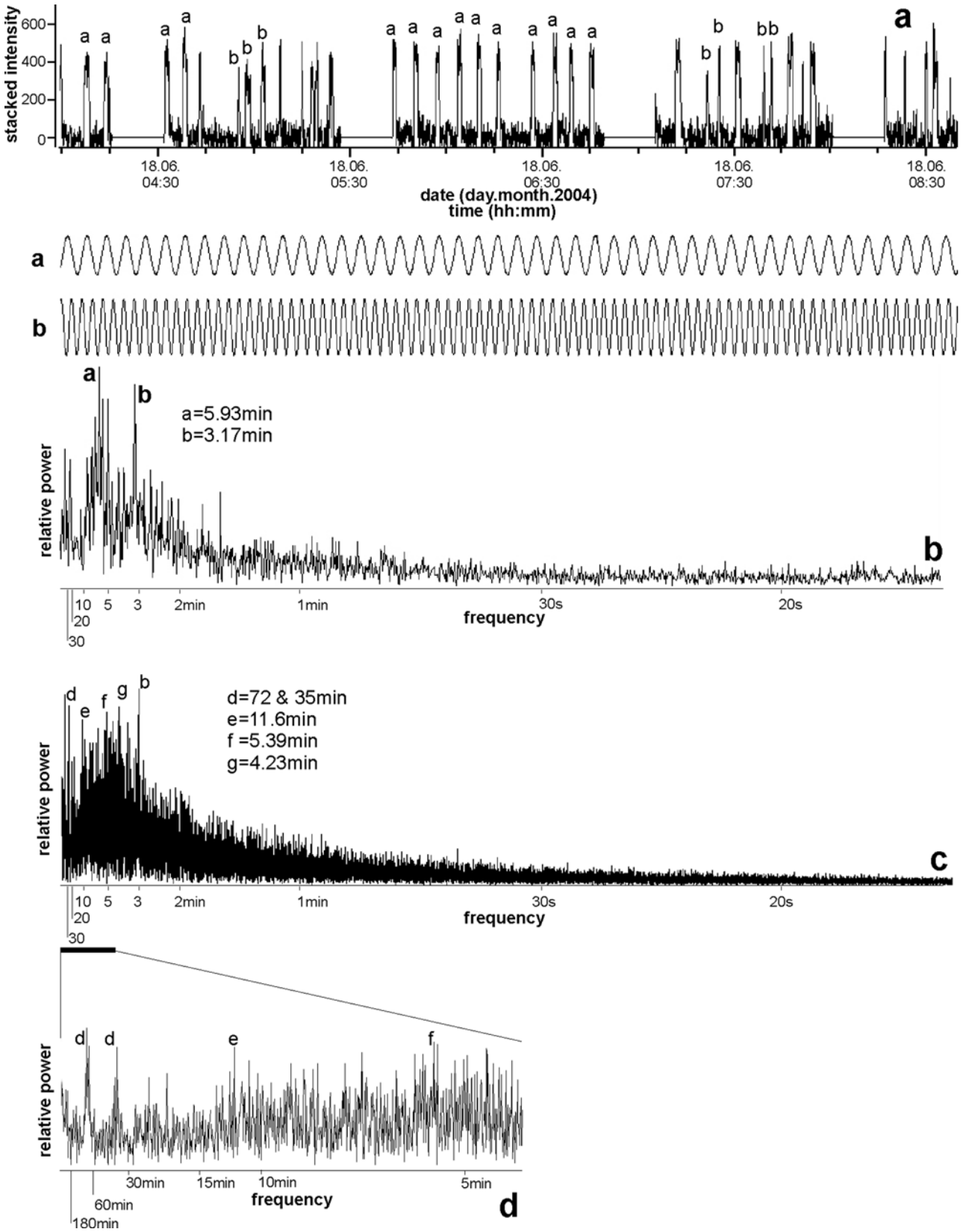

Figure 14. Spectrum analysis of seep 6. (a) A subset of the entire trace with a series of regularly occurring bubble releases. (b) The respective power spectrum, highlighting two dominant frequencies (frequencies a and b). (c) The entire data set as shown in Figure 6 was used to calculate the power spectrum, enlarged in Figure 14d. The frequencies labeled d (72 and 35 min) are caused by the recording setting of ~1 h pinging and ~15 min pause.

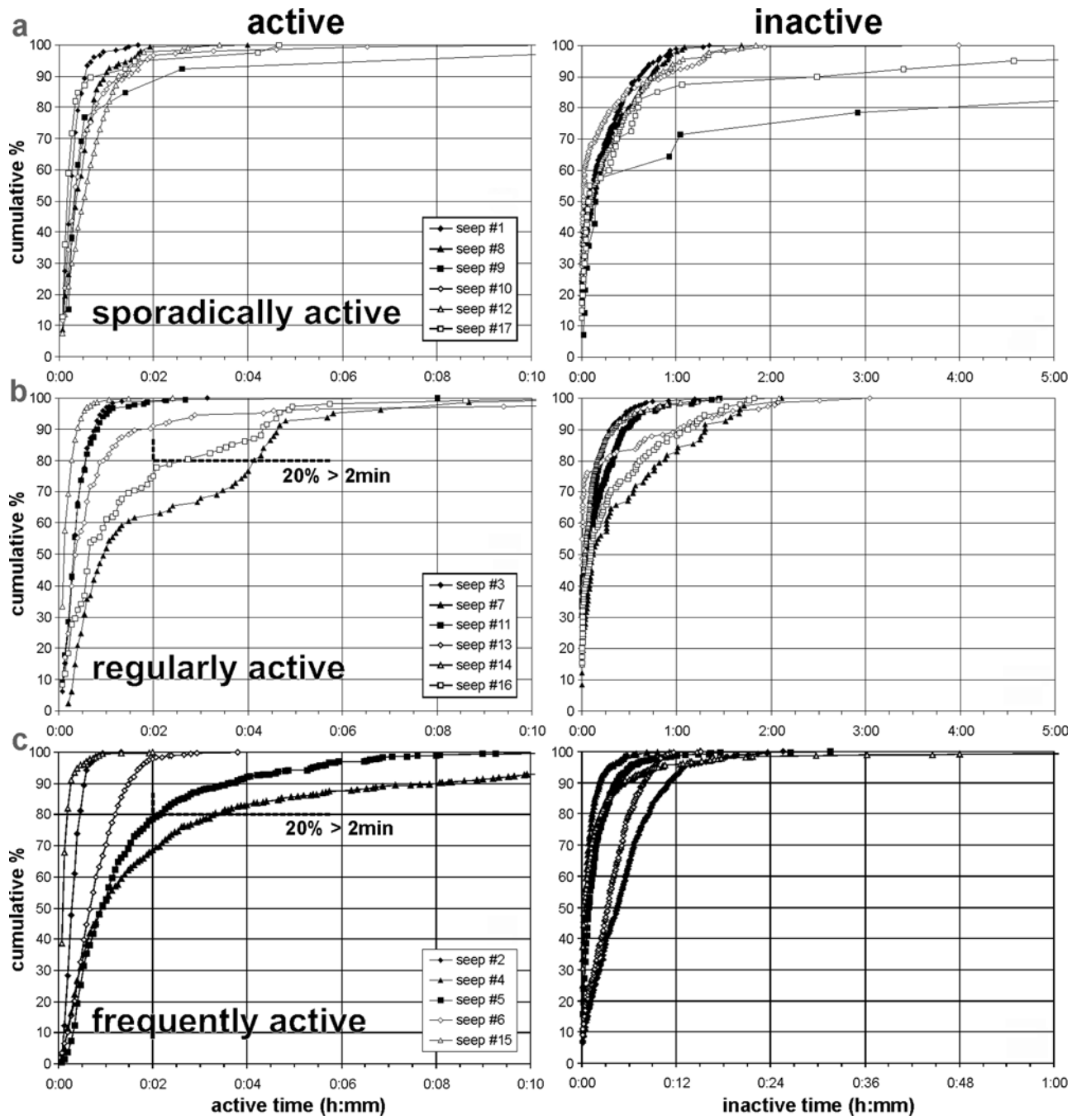

Figure 15. Cumulative percentage curves depicting the length of active (left) and inactive (right) periods for all seeps grouped into (a) sporadically, (b) regularly, and (c) frequently active seeps. Active periods lasting longer than 2 min are an exception for most of the seeps. Only at four seeps 20% of the release events last longer than 2 min (seeps 4, 5, 7, and 16). As no filtering was applied, many short inactive periods occur as short interruptions of a longer bubble release event (see also mode of inactive periods in Table 1). Note that the *x* axis scale in the right panel of Figure 15c is different from that in the right panels of Figures 15a and 15b.

bursts (>350) or where active for more than 20% of the observation time. The burst length was typically around one minute. For some seeps a very periodic release could be observed within a time range of 2–3 h. Only one seep was active for 75% of the observation time and one for 45%. All others were active for less than 20% with an average for all seeps of only 12%.

[51] The great variability of the bubble release activity also makes it advisable to use direct flux measurements at single seeps for flux extrapolation in time and space with great caution. Both tremendous underestimates and overestimates of gas fluxes are possible without having an idea of the temporal variability of the activity of the respective seep.

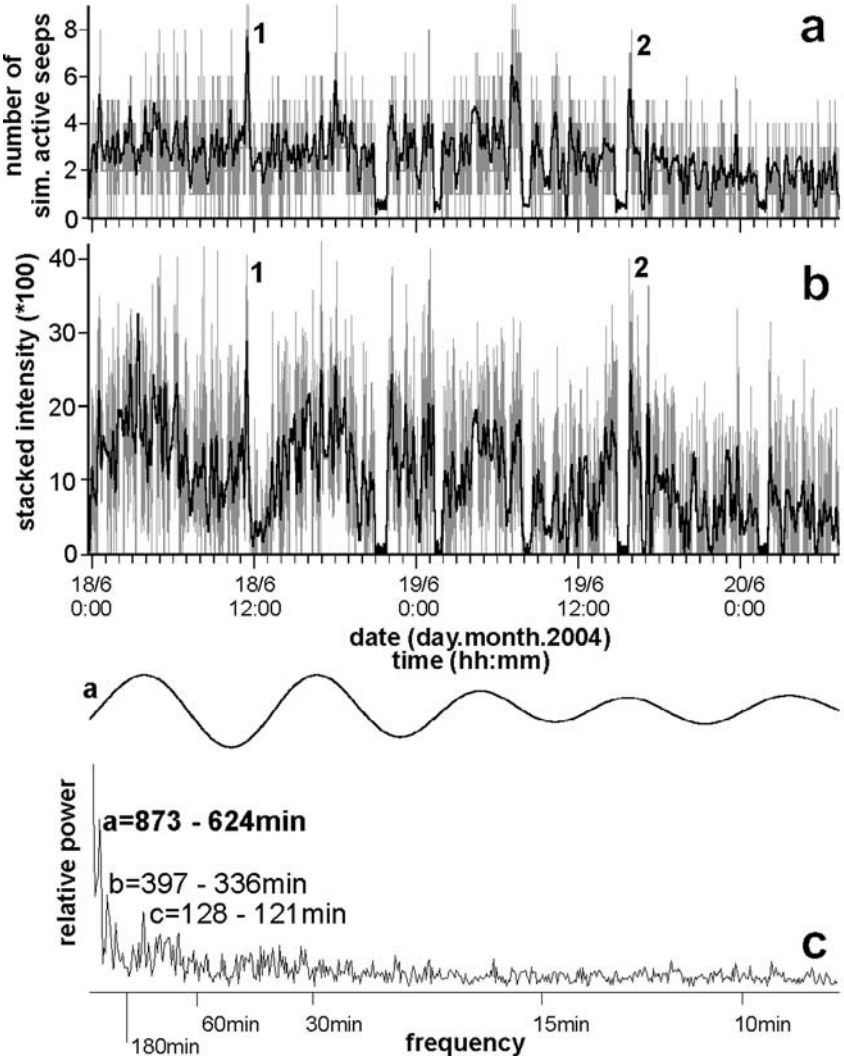

Figure 16. Activity analyses of the entire seep area using (a) the changing number of simultaneously active seeps and (b) the integrated strength of the recorded signal (stacked intensity) at the time the seeps have been active. Grey data are raw data and black lines are data derived from low-pass filtering. (c) Power spectrum of the stacked intensities of Figure 16b. The spectrum indicates three stronger frequencies, whereas frequency a is similar to the frequency of the most active seep 4.

[52] During the processing it became obvious that the used pinging/pause setting for the data recording complicates data processing and FFT analyses in particular. After the deployment this setting has been avoided. Furthermore, having water current measurements for the same time period as the GasQuant recording would provide additional proof that the shift of bubbles in the swath plane is indeed current induced. Upward looking ADCPs with 75 and 300 kHz were successfully tested to run parallel with GasQuant without acoustic interferences and attaching an ADCP to the lander is now standard procedure for GasQuant deployments.

[53] **Acknowledgments.** Thanks go to L3 Communications ELAC-Nautik GmbH, Kiel, Germany, for the great support developing and modifying the GasQuant system. This is publication GEOTECH - 245 of the R&D-Programme GEOTECHNOLOGIEN funded by the German Ministry of Education and Research (BMBF) and German Research Foundation (DFG) with grants for the LOTUS (03G0565) and the COMET (03G0600D) projects. Warm thanks go to the crew of RV *Vodyanitsky* (Sevastopol, Ukraine) for their enthusiasm and great help with deploying and particularly recovering the GasQuant lander. More warm thanks go to the technicians and involved scientists at IFM-GEOMAR: Peter Linke, Martin Pieper, Bernhard Bannert, Wolfgang Queisser, and Michael Poser. Funding for the Black Sea cruise was provided by the EU-funded project CRIMEA (EVK-2-CT-2002-00162). Furthermore, the EU supported the author with a Marie Curie OIF grant (MOIF-CT-2005-007436) during the time the manuscript was written. Finally, thanks go to Jens Schneider and Peter Staelens for discussions and to two reviewers who provided useful comments on an earlier version of this manuscript.

References

Dickens, G. R., J. R. O'Neil, D. K. Rea, and R. M. Owen (1995), Dissociation of oceanic methane hydrate as a cause of the carbon isotope excursion at the end of the Paleocene, *Paleoceanography*, *10*(6), 965–971, doi:10.1029/95PA02087.

Dimitrov, L. I. (2002), Mud volcanoes—The most important pathway for degassing deeply buried sediments, *Earth Sci. Rev.*, *59*(1–4), 49–76, doi:10.1016/S0012-8252(02)00069-7.

Greinert, J., and B. Nützel (2004), Hydroacoustic experiments to establish a method for the determination of methane bubble fluxes at cold seeps, *Geo Mar. Lett.*, *24*, 75–85, doi:10.1007/s00367-003-0165-7.

Greinert, J., Y. Artemov, V. Egorov, M. De Batist, and D. McGinnis (2006), 1300-m-high rising bubbles from mud volcanoes at 208 0 m in the Black Sea: Hydroacoustic characteristics and temporal variability, *Earth Planet. Sci. Lett.*, *244*(1–2), 1–15, doi:10.1016/j.epsl.2006.02.011.

Heeschen, K. U., A. M. Trehu, W. C. Collier, E. Suess, and G. Rehder (2003), Distribution and height of methane bubbles plumes on the Cascadia Margin characterized by acoustic imaging, *Geophys. Res. Lett.*, *30*(12), 1643, doi:10.1029/2003GL016974.

Hornafius, J. S., D. Quigley, and B. P. Luyendyk (1999), The world's most spectacular marine hydrocarbon seeps (Coal Oil Point, Santa Barbara Channel, California): Quantification of emission, *J. Geophys. Res.*, *104*, 20,703–20,711, doi:10.1029/1999JC900148.

Kennett, J. P., K. G. Cannariato, I. L. Hendy, and R. J. Behl (2003), *Role of Methane Hydrates in Late Quaternary Climatic Change: The Clathrate Gun Hypothesis*, *Spec. Publ. Ser.*, vol. 54, 216 pp., AGU, Washington, D. C.

Leifer, I., and A. Judd (2002), Oceanic methane layers: The hydrocarbon seep bubble deposition hypothesis, *Terra Nova*, *14*, 417–424, doi:10.1046/j.1365-3121.2002.00442.x.

Leifer, I., and I. R. MacDonald (2003), Dynamics of the gas flux from shallow gas hydrate deposits: Interaction between oily hydrate bubbles and the oceanic environment, *Earth Planet. Sci. Lett.*, *210*, 411–424, doi:10.1016/S0012-821X(03)00173-0.

Leifer, I., and K. Patro (2002), The bubble mechanism for methane transport from the shallow sea bed to the surface: A review and sensitivity study, *Cont. Shelf Res.*, *22*, 2409–2428, doi:10.1016/S0278-4343(02)00065-1.

Leifer, I., J. R. Boles, B. P. Luyendyk, and J. F. Clark (2004), Transient discharges from marine hydrocarbon seeps: Spatial and temporal variability, *Environ. Geol.*, *46*, 1038–1052, doi:10.1007/s00254-004-1091-3.

Leifer, I., B. P. Luyendyk, J. Boles, and J. F. Clark (2006), Natural marine seepage blowout: Contribution to atmospheric methane, *Global Biogeochem. Cycles*, *20*, GB3008, doi:10.1029/2005GB002668.

Linke, P., O. Pfannkuche, M. E. Torres, R. W. Collier, U. Witte, J. McManus, D. E. Hammond, K. M. Brown, M. D. Tryon, and K. Nakamura (1999), Variability of benthic flux and discharge rates at vent sites determined by in situ instruments, *Eos Trans. AGU*, *80*, 509.

MacDonald, I. R., L. C. Bender, M. Vardaro, B. Bernard, and J. M. Brooks (2005), Thermal and visual time-series at a seafloor gas hydrate deposit on the Gulf of Mexico slope, *Earth Planet. Sci. Lett.*, *233*, 45–59, doi:10.1016/j.epsl.2005.02.002.

McGinnis, D. F., J. Greinert, Y. Artemov, S. E. Beaubien, and A. Wüest (2006), Fate of rising methane bubbles in stratified waters: How much methane reaches the atmosphere?, *J. Geophys. Res.*, *111*, C09007, doi:10.1029/2005JC003183.

Medwin, H., and C. S. Clay (1998), *Fundamentals in Acoustic Oceanography*, 712 pp., Academic Press, San Diego, Calif.

Naudts, L., J. Greinert, Y. Artemov, P. Staelens, J. Poort, P. Van Rensbergen, and M. De Batist (2006), Geological and morphological setting of 2778 methane seeps in the Dnepr paleo-delta, northwestern Black Sea, *Mar. Geol.*, *227*(3–4), 177–199, doi:10.1016/j.margeo.2005.10.005.

Naudts, L., J. Greinert, Y. Artemov, S. Beaubien, C. Borowski, and M. De Batist (2008), Abnormally high acoustic sea-floor backscattering in active methane venting areas, Dnepr paleo-delta, northwestern Black Sea, *Mar. Geol.*, *251*, 253–267.

Norris, D. R., and U. Röhl (1999), Carbon cycling and chronology of climate warming during the Palaeocene/Eocene transition, *Nature*, *401*, 775–778, doi:10.1038/44545.

Obzhirov, A., R. Shakirov, A. Salyuk, E. Suess, N. Biebow, and A. Salomatin (2004), Relations between methane venting, geological structure and seismo-tectonics in the Okhotsk Sea, *Geo Mar. Lett.*, *24*, 135–139, doi:10.1007/s00367-004-0175-0.

Pfannkuche, O., and P. Linke (2003), GEOMAR Landers as long-term deep-sea observatories, *Sea Technol.*, *44*, 50–55.

Polikarpov, G. G., V. N. Egorov, A. I. Nezhdanonv, S. B. Gulin, Y. D. Kulev, and M. B. Gulin (1989), Methane gas seeps in the Black Sea-A new object of molismology, in *Molismology of the Black Sea*, edited by G. G. Polikarpov et al., pp. 10–20, Nauka, Kiev.

Quigley, D. C., J. S. Hornafius, B. P. Luyendyk, R. D. Francis, J. Clark, and L. Washburn (1999), Decrease in natural marine hydrocarbon seepage near Coal Oil Point, California, associated with offshore oil production, *Geology*, *27*(11), 1047–1050, doi:10.1130/0091-7613(1999)027<1047:DINMHS>2.3.CO;2.

Sauter, E. J., S. I. Muyakshin, J.-L. Charlou, M. Schlüter, A. Boetius, K. Jerosch, E. Damm, J.-P. Foucher, and M. Klages (2006), Methane discharge from a deep-sea submarine mud volcano into the upper water column by gas hydrate-coated methane bubbles, *Earth Planet. Sci. Lett.*, *243*, 354–365, doi:10.1016/j.epsl.2006.01.041.

Smith, S. W. (2002), *Digital Signal Processing: A Practical Guide for Engineers and Scientists*, 672 pp., Newnes, London.

Suess, E., et al. (1999), Gas hydrate destabilization: Enhanced dewatering, benthic material turnover and large methane plumes at the Cascadia convergent margin, *Earth Planet. Sci. Lett.*, *170*, 1–15, doi:10.1016/S0012-821X(99)00092-8.

Torres, M. E., J. McManus, D. E. Hammond, M. A. de Angelis, K. U. Heeschen, S. L. Colbert, M. D. Tryon, K. M. Brown, and E. Suess (2002), Fluid and chemical fluxes in and out of sediments hosting methane hydrate deposits on Hydrate Ridge, OR, I: Hydrological provinces, *Earth Planet. Sci. Lett.*, *201*, 525–540, doi:10.1016/S0012-821X(02)00733-1.

Tryon, D., K. M. Brown, M. E. Torres, A. M. Trehu, J. McManus, and R. W. Collier (1999), Measurements of transience and downward fluid flow near episodic methane gas vents, Hydrate Ridge, Cascadia, *Geology*, *27*, 1075–1078, doi:10.1130/0091-7613(1999)027<1075:MOTADF>2.3.CO;2.

Tryon, M. D., K. M. Brown, and M. E. Torres (2002), Fluid and chemical flux in and out of sediments hosting methane hydrate deposits on Hydrate Ridge, OR, II: Hydrological processes, *Earth Planet. Sci. Lett.*, *201*, 541–557, doi:10.1016/S0012-821X(02)00732-X.

Van Rensbergen, P., M. De Batist, J. Klerkx, R. Hus, J. Poort, M. Vanneste, N. Granin, O. Khlystov, and P. Krinitsky (2002), Sublacustrine mud volcanoes and methane seeps caused by dissociation of gas hydrates in Lake Baikal, *Geology*, *30*, 631–634, doi:10.1130/0091-7613(2002)030<0631:SMVAMS>2.0.CO;2.

Wever, T. F., R. Lühder, H. Voh, and U. Knispel (2006), Potential environmental control of free shallow gas in the seafloor of Eckernförde Bay, Germany, *Mar. Geol.*, *225*, 1–4, doi:10.1016/j.margeo.2005.08.005.

J. Greinert, Renard Centre of Marine Geology, Ghent University, Krijgslaan 281 s8, B-9000 Gent, Belgium. (greinert@nioz.nl)